Polarization-resolved time-delay signatures of chaos induced by FBG-feedback in VCSEL

Zhu-Qiang Zhong,[1] Song-Sui Li,[2] Sze-Chun Chan,[2,3] Guang-Qiong Xia,[1] and Zheng-Mao Wu[1,*]

[1] *School of Physical Science and Technology, Southwest University, Chongqing 400715, China*
[2] *Department of Electronic Engineering, City University of Hong Kong, Hong Kong, China*
[3] *State Key Laboratory of Millimeter Waves, City University of Hong Kong, Hong Kong, China*
**zmwu@swu.edu.cn*

Abstract: Polarization-resolved chaotic emission intensities from a vertical-cavity surface-emitting laser (VCSEL) subject to feedback from a fiber Bragg grating (FBG) are numerically investigated. Time-delay (TD) signatures of the feedback are examined through various means including self-correlations of intensity time-series of individual polarizations, cross-correlation of intensities time-series between both polarizations, and permutation entropies calculated for the individual polarizations. The results show that the TD signatures can be clearly suppressed by selecting suitable operation parameters such as the feedback strength, FBG bandwidth, and Bragg frequency. Also, in the operational parameter space, numerical maps of TD signatures and effective bandwidths are obtained, which show regions of chaotic signals with both wide bandwidths and weak TD signatures. Finally, by comparing with a VCSEL subject to feedback from a mirror, the VCSEL subject to feedback from the FBG generally shows better concealment of the TD signatures with similar, or even wider, bandwidths.

OCIS codes: (140.5960) Semiconductor lasers; (190.3100) Instabilities and chaos.

References and links

1. R. Lang and K. Kobayashi, "External optical feedback effects on semiconductor injection laser properties," IEEE J. Quantum Electron. **16**(3), 347–355 (1980).
2. J. Mork, B. Tromborg, and J. Mark, "Chaos in semiconductor lasers with optical feedback: theory and experiment," IEEE J. Quantum Electron. **28**(1), 93–108 (1992).
3. I. Fischer, O. Hess, W. Elsa, and E. Göbel, "High-dimensional chaotic dynamics of an external cavity semiconductor laser," Phys. Rev. Lett. **73**(16), 2188–2191 (1994).
4. R. Vicente, J. Daudén, P. Colet, and R. Toral, "Analysis and characterization of the hyperchaos generated by a semiconductor laser subject to a delayed feedback loop," IEEE J. Quantum Electron. **41**(4), 541–548 (2005).
5. M. W. Lee, P. Rees, K. A. Shore, S. Ortin, L. Pesquera, and A. Valle, "Dynamical characterisation of laser diode subject to double optical feedback for chaotic optical communications," IEE Proc., Optoelectron. **152**(2), 97–102 (2005).
6. D. Rontani, A. Locquet, M. Sciamanna, and D. S. Citrin, "Loss of time-delay signature in the chaotic output of a semiconductor laser with optical feedback," Opt. Lett. **32**(20), 2960–2962 (2007).
7. J. Ohtsubo, "Chaos synchronization and chaotic signal masking in semiconductor lasers with optical feedback," IEEE J. Quantum Electron. **38**(9), 1141–1154 (2002).
8. A. Argyris, D. Syvridis, L. Larger, V. Annovazzi-Lodi, P. Colet, I. Fischer, J. García-Ojalvo, C. R. Mirasso, L. Pesquera, and K. A. Shore, "Chaos-based communications at high bit rates using commercial fibre-optic links," Nature **438**(7066), 343–346 (2005).
9. C. H. Cheng, Y. C. Chen, and F. Y. Lin, "Chaos time delay signature suppression and bandwidth enhancement by electrical heterodyning," Opt. Express **23**(3), 2308–2319 (2015).
10. A. Uchida, K. Amano, M. Inoue, K. Hirano, S. Naito, H. Someya, I. Oowada, T. Kurashige, M. Shiki, S. Yoshimori, K. Yoshimura, and P. Davis, "Fast physical random bit generation with chaotic semiconductor lasers," Nat. Photonics **2**(12), 728–732 (2008).
11. I. Kanter, Y. Aviad, I. Reidler, E. Cohen, and M. Rosenbluh, "An optical ultrafast random bit generator," Nat. Photonics **4**(1), 58–61 (2010).

#238400 - $15.00 USD Received 20 Apr 2015; revised 29 May 2015; accepted 30 May 2015; published 3 Jun 2015

12. D. Rontani, A. Locquet, M. Sciamanna, D. S. Citrin, and S. Ortin, "Time-Delay identification in a chaotic semiconductor laser with optical feedback: a dynamical point of view," IEEE J. Quantum Electron. **45**(7), 879–891 (2009).
13. J. G. Wu, Z. M. Wu, X. Tang, X. D. Lin, T. Deng, G. Q. Xia, and G. Y. Feng, "Simultaneous generation of two sets of time delay signature eliminated chaotic signals by using mutually coupled semiconductor lasers," IEEE Photon. Technol. Lett. **23**(12), 759–761 (2011).
14. J. G. Wu, Z. M. Wu, G. Q. Xia, and G. Y. Feng, "Evolution of time delay signature of chaos generated in a mutually delay-coupled semiconductor lasers system," Opt. Express **20**(2), 1741–1753 (2012).
15. S. S. Li, Q. Liu, and S. C. Chan, "Distributed feedbacks for time-delay signature suppression of chaos generated from a semiconductor laser," IEEE Photon. J. **4**(5), 1930–1935 (2012).
16. S. S. Li and S. C. Chan, "Chaotic time-delay signature suppression in a semiconductor laser with frequency-detuned grating feedback," IEEE J. Sel. Top. Quantum Electron. **99**, 1 (2015).
17. K. Iga, "Surface-emitting laser—its birth and generation of new optoelectronics field," IEEE J. Sel. Top. Quantum Electron. **6**(6), 1201–1215 (2000).
18. R. Ju, P. S. Spencer, and K. A. Shore, "Polarization-preserved and polarization-rotated synchronization of chaotic vertical-cavity surface-emitting lasers," IEEE J. Quantum Electron. **41**(12), 1461–1467 (2005).
19. K. Panajotov, M. Sciamanna, M. A. Arteaga, and H. Thienpont, "Optical feedback in vertical-cavity surface-emitting lasers," IEEE J. Sel. Top. Quantum Electron. **19**(4), 1700312 (2013).
20. F. Koyama, "Recent advance of VCSEL photonics," J. Lightwave Technol. **24**(12), 4502–4513 (2006).
21. S. Y. Xiang, W. Pan, B. Luo, L. S. Yan, X. H. Zou, N. Jiang, L. Yang, and H. Zhu, "Conceal time-delay signature of chaotic vertical-cavity surface-emitting lasers by variable-polarization optical feedback," Opt. Commun. **284**(24), 5758–5765 (2011).
22. N. Q. Li, W. Pan, B. Luo, L. S. Yan, X. Zou, M. Xu, N. Jiang, S. Xiang, and P. Mu, "Numerical characterization of time delay signature in chaotic vertical-cavity surface-emitting lasers with optical feedback," Opt. Commun. **285**(18), 3837–3848 (2012).
23. S. Priyadarshi, Y. H. Hong, I. Pierce, and K. A. Shore, "Experimental investigations of time-delay signature concealment in chaotic external cavity VCSELs subject to variable optical polarization angle of feedback," IEEE J. Sel. Top. Quantum Electron. **19**(4), 1700707 (2013).
24. H. Lin, Y. H. Hong, and K. A. Shore, "Experimental study of time-delay signatures in vertical-cavity surface-emitting lasers subject to double-cavity polarization-rotated optical feedback," J. Lightwave Technol. **32**(9), 1829–1836 (2014).
25. Y. H. Hong, P. S. Spencer, and K. A. Shore, "Wideband chaos with time-delay concealment in vertical-cavity surface-emitting lasers with optical feedback and injection," IEEE J. Quantum Electron. **50**(4), 236–242 (2014).
26. P. Xiao, Z. M. Wu, J. G. Wu, L. Jiang, T. Deng, X. Tang, L. Fan, and G. Q. Xia, "Time-delay signature concealment of chaotic output in a vertical-cavity surface-emitting laser with double variable-polarization optical feedback," Opt. Commun. **286**, 339–343 (2013).
27. Z. Q. Zhong, Z. M. Wu, J. G. Wu, and G. Q. Xia, "Time-delay signature suppression of polarization-resolved chaos outputs from two mutually coupled VCSELs," IEEE Photon. J. **5**(2), 1500409 (2013).
28. Y. Li, Z. M. Wu, Z. Q. Zhong, X. J. Yang, S. Mao, and G. Q. Xia, "Time-delay signature of chaos in 1550 nm VCSELs with variable-polarization FBG feedback," Opt. Express **22**(16), 19610–19620 (2014).
29. J. Liu, Z. M. Wu, and G. Q. Xia, "Dual-channel chaos synchronization and communication based on unidirectionally coupled VCSELs with polarization-rotated optical feedback and polarization-rotated optical injection," Opt. Express **17**(15), 12619–12626 (2009).
30. M. S. Miguel, Q. Feng, and J. V. Moloney, "Light-polarization dynamics in surface-emitting semiconductor lasers," Phys. Rev. A **52**(2), 1728–1739 (1995).
31. I. Gatare, M. Sciamanna, A. Locquet, and K. Panajotov, "Influence of polarization mode competition on the synchronization of two unidirectionally coupled vertical-cavity surface-emitting lasers," Opt. Lett. **32**(12), 1629–1631 (2007).
32. T. Erdogan, "Fiber grating spectra," J. Lightwave Technol. **15**(8), 1277–1294 (1997).
33. C. Bandt and B. Pompe, "Permutation entropy: a natural complexity measure for time series," Phys. Rev. Lett. **88**(17), 174102 (2002).
34. M. C. Soriano, L. Zunino, O. A. Rosso, I. Fischer, and C. R. Mirasso, "Time scales of a chaotic semiconductor laser with optical feedback under the lens of a permutation information analysis," IEEE J. Quantum Electron. **47**(2), 252–261 (2011).
35. J. Martin-Regalado, F. Prati, M. San Miguel, and N. B. Abraham, "Polarization properties of vertical-cavity surface-emitting lasers," IEEE J. Quantum Electron. **33**(5), 765–783 (1997).
36. F. Y. Lin, Y. K. Chao, and T. C. Wu, "Effective bandwidths of broadband chaotic signals," IEEE J. Quantum Electron. **48**(8), 1010–1014 (2012).
37. Y. Hong, "Experimental study of time-delay signature of chaos in mutually coupled vertical-cavity surface-emitting lasers subject to polarization optical injection," Opt. Express **21**(15), 17894–17903 (2013).

1. Introduction

External cavity feedback (ECF) is the most commonly used technique to drive a semiconductor laser (SL) into chaotic states [1–9]. The chaotic output from an ECF-SL typically contains

#238400 - $15.00 USD Received 20 Apr 2015; revised 29 May 2015; accepted 30 May 2015; published 3 Jun 2015

obvious signatures of the time-delay (TD) originating from the optical round trip between the laser and the external feedback mirror [5, 6]. Such TD signatures of chaos can potentially compromise the security in optical chaos encryption systems [7–9]. They also limit the tunability of the bit rates in high-speed random bit sequences [10, 11]. The suppression of the TD signature, therefore, has become very important for chaos generations in ECF-SLs.

A number of theoretical and experimental investigations have been conducted to suppress the TD signatures in edge-emitting SLs. Rontani *et al.* reported the elimination of TD signatures at relatively low feedback rates when the delay is close to the inverse of the relaxation resonance frequency [6, 12]. Lee *et al.* demonstrated the possibility to obscure the TD signatures by introducing another external cavity to realize a double-ECF [5]. We also investigated the TD signatures in two mutually coupled SLs in which each SL can be regarded as an active nonlinear reflector to the other SL, where experimental and numerical results both show simultaneous elimination of TD signatures from the two SLs [13, 14]. Besides, ECF using a fiber Bragg grating (FBG) as a distributed reflector was also reported for suppressing the TD signatures [15, 16]. With the success of these approaches in the edge-emitting SLs, their extensions to the vertical-cavity surface-emitting lasers (VCSELs) have started to attract much attention. This is due to the many unique advantages offered by VCSELs which include being low cost, possessing low threshold currents, yielding circular output beams of narrow divergence, allowing large-scale integration into two-dimensional arrays, and supporting single longitudinal-mode operation due to the short cavity lengths [17–20].

Recently, much effort has been made to suppress the chaotic TD signatures in ECF-VCSELs [21–26]. Xiang *et al*. proposed concealing the TD signatures in VCSELs though invoking chaos by variable-polarization optical feedback [21]. Li *et al*. numerically investigated the TD signatures of chaos in VCSELs with optical feedback [22]. Priyadarshi *et al.* reported experiments that verified the scheme [23]. Lin *et al*. considered adding one more feedback to realize a double-cavity polarization-rotated optical feedback into a VCSEL [24]. Hong *et al*. experimentally compared a number of combinations utilizing two VCSELs [25]. It was found that, when an ECF-VCSEL is mutually or unidirectionally coupled to the other VCSEL, simultaneous suppression of TD signatures and enhancement of chaotic bandwidth can be obtained. We also studied similar TD signature suppression in a chaotic VCSEL that is subject to two feedbacks with variable polarizations [26] or is subject to mutual coupling from another VCSEL [27]. Additionally, we investigated the TD features of a chaotic VCSEL under variable-polarization feedback from a grating [28], but only the total output intensity was considered without resolving the two polarization components (PCs). This was due to the challenge of operating the VCSEL with two co-existing PCs in chaos. However, a chaotic VCSEL with two simultaneously co-existing PCs can enable applications such as dual-channel chaos communication and a dual-polarization high-speed random bit generator [29].

In this paper, we numerically investigate the polarization-resolved TD features in a VCSEL subject to feedback from a FBG with no need for polarization rotation. When the operation parameters are carefully selected, the VCSEL is found to emit chaotic outputs with two orthogonal linear PCs. The PCs are emitted simultaneously, but the two PCs carry two different waveforms. From the intensity time-series, the TD signatures are thoroughly examined using self-correlations of individual PCs, cross-correlations between the two PCs, and permutation entropies calculated from the individual PCs. The TD signatures are shown to be much reduced as compared to using mirror instead of FBG for the feedback. Then, in the parameter space of the feedback rate and frequency deviation, numerical maps are obtained in revealing regions of chaotic signals with both wide bandwidths and small TD signatures. Lastly, when compared to the conventional ECF-VCSEL using a mirror, the feedback from the FBG is found to generally show better concealment of the TD signatures, illustrating the benefits of using FBG feedback on the VCSEL.

#238400 - $15.00 USD Received 20 Apr 2015; revised 29 May 2015; accepted 30 May 2015; published 3 Jun 2015

2. System model and theory

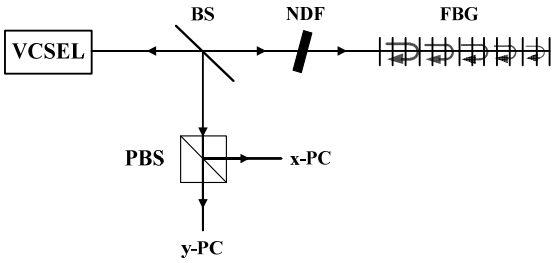

Fig. 1. Schematic diagram of a polarization-resolved monitoring of a VCSEL under FBG feedback. VCSEL: vertical-cavity surface-emitting laser; BS: beamsplitter; NDF: neutral density filter; FBG: fiber Bragg grating; PBS: polarization beam splitter.

Figure 1 shows the schematic diagram of a VCSEL subject to polarization-preserved feedback from a FBG. The output from the VCSEL is split by a beam splitter (BS) into two parts. One part is reflected by the FBG and fed back to the VCSEL with a time delay and with a feedback strength controlled by a neutral density filter (NDF). The other part is sent to a polarizing beam splitter (PBS) and then split into two PCs in *x*- and *y*- directions, respectively. In this work, we focus on the polarization-resolved nonlinear dynamics of VCSELs. Under this case, the spin-flip model (SFM) [30, 31], in which the phase relationship between *x*- and *y*-PCs has been taken into account, is more suitable compared with the two-mode model [19]. The rate equations for the VCSEL of Fig. 1 are:

$$\frac{dE_x}{dt} = \kappa(1+i\alpha)\left[(N-1)E_x + inE_y\right] - \left(\gamma_a + i\gamma_p - i2\pi f_m\right)E_x + \eta e^{-i\theta} r(t) * E_x(t-\tau) \quad (1)$$

$$\frac{dE_y}{dt} = \kappa(1+i\alpha)\left[(N-1)E_y - inE_x\right] + \left(\gamma_a + i\gamma_p + i2\pi f_m\right)E_y + \eta e^{-i\theta} r(t) * E_y(t-\tau) \quad (2)$$

$$\frac{dN}{dt} = \gamma(\mu - N) - \gamma N\left(|E_x|^2 + |E_y|^2\right) + i\gamma n\left(E_x E_y^* - E_y E_x^*\right) \quad (3)$$

$$\frac{dn}{dt} = -\gamma_s n - \gamma n\left(|E_x|^2 + |E_y|^2\right) + i\gamma N\left(E_x E_y^* - E_y E_x^*\right) \quad (4)$$

Here, the subscripts *x* and *y* denote the *x*-PC and *y*-PC, respectively. *E* is the slowly-varying complex amplitude of the optical electric field. *N* accounts for the normalized total carrier population inversion in excess of its transparency value. *n* accounts for the difference in carrier inversions between opposite spins. κ is the photon decay rate. γ is the carrier decay rate. γ_s is the spin homogenization rate. γ_a is the linear cavity dichroism. γ_p is the linear phase anisotropy. α is the linewidth enhancement factor. μ is the normalized injection current. f_m ($= f_0 - f_{\mathrm{FBG}}$, where f_0 is the mean frequency of the two PCs in the free-running VCSEL and f_{FBG} is the Bragg frequency of the FBG) is the frequency deviation. η is the feedback rate. τ is the group delay of the round-trip feedback in exclusion of the FBG. θ specifies the phase of the optical feedback along with the impulse response $r(t)$ of the FBG. The impulse response is given by the inverse Fourier transform of the frequency response of the FBG:

$$r(\Omega) = \frac{\kappa_B \sinh\left(\sqrt{\kappa_B^2 - \delta^2}L\right)}{-\delta \sinh\left(\sqrt{\kappa_B^2 - \delta^2}L\right) + i\sqrt{\kappa_B^2 - \delta^2}\cosh\left(\sqrt{\kappa_B^2 - \delta^2}L\right)} \quad (5)$$

#238400 - $15.00 USD Received 20 Apr 2015; revised 29 May 2015; accepted 30 May 2015; published 3 Jun 2015

where κ_B is the magnitude of the coupling coefficient of the FBG, L is the length of the FBG, δ is the phase mismatch between the counterpropagating modes that equals $n_g\Omega/c$ with n_g and c being the group index of the fiber and the speed of light in vacuum, respectively. A uniform single-mode FBG is assumed due to its relatively simple structure. Its reflection bandwidth can be approximated by $c\kappa_B/\pi n_g$ when it is highly reflective at the Bragg frequency [32]. The feedback from the FBG reduces to that from a mirror when κ_B goes to infinity. The rate Eqs. (1)-(4) are solved numerically by using the fourth-order Runge-Kutta algorithm. The time step is fixed at $\delta t = 2$ ps. The laser parameters are chosen as [31]: $\kappa = 300$ ns^{-1},$\gamma = 1$ ns^{-1}, $\gamma_s = 50$ ns^{-1}, $\gamma_a = 0.1$ ns^{-1}, $\gamma_p = 10$ ns^{-1}, $\alpha = 3$, and $\mu = 2.7$. The feedback is specified by [15]: $\tau = 3$ ns, $n_g = 1.45$, $\theta = 0$, $\kappa_B = 100$ m^{-1}, and $L = 20$ mm.

The following sections focus on the output intensities of the VCSEL, which are numerically represented by $I_x(t) = |E_x(t)|^2$ and $I_y(t) = |E_y(t)|^2$ for the x- and y-PCs, respectively. Even when the VCSEL is driven into chaos, the residual information of the value of τ could be hidden in the intensities. Such signatures of the TD can possibly be extracted by different correlations of the intensity time-series. The self-correlation functions (SFs) are respectively defined for the x- and y-PCs as [6, 13]:

$$C_{xx}(\Delta t) = \frac{\left\langle \left(I_x(t+\Delta t) - \langle I_x \rangle\right)\left(I_x(t) - \langle I_x \rangle\right)\right\rangle}{\left\langle \left(I_x - \langle I_x \rangle\right)^2 \right\rangle} \tag{6}$$

$$C_{yy}(\Delta t) = \frac{\left\langle \left(I_y(t+\Delta t) - \langle I_y \rangle\right)\left(I_y(t) - \langle I_y \rangle\right)\right\rangle}{\left\langle \left(I_y - \langle I_y \rangle\right)^2 \right\rangle} \tag{7}$$

and the cross-correlation function (XF) between the x- and y-PCs is defined as:

$$C_{xy}(\Delta t) = \frac{\left\langle \left(I_x(t+\Delta t) - \langle I_x \rangle\right)\left(I_y(t) - \langle I_y \rangle\right)\right\rangle}{\sqrt{\left\langle \left(I_x - \langle I_x \rangle\right)^2 \right\rangle \left\langle \left(I_y - \langle I_y \rangle\right)^2 \right\rangle}} \tag{8}$$

where $\langle\cdot\rangle$ denotes time-average and Δt is the time-shift.

Also, TD information can possibly be revealed by the permutation entropy (PE) [21, 28, 33, 34]. PE is evaluated versus the embedding delay time τ_e by the following procedure for each polarization with intensity time series $I(t)$. A set of D-dimensional vectors ($I(m\delta t + \tau_e)$, $I(m\delta t + 2\tau_e)$, …, $I(m\delta t + D\tau_e)$) is formed for all integral index m in the simulation. Every vector belongs to one particular order permutation for the D intensities, amongst the total of $D!$ possible permutations. For a permutation labeled as π, its number of occurrences is denoted by $p(\pi)$, which is normalized to the total number of the vectors. PE is then defined as:

$$H(\tau_e) = -\sum p(\pi) \log_{D!} p(\pi) \tag{9}$$

where the summation is performed over all $D!$ possible π. Throughout this paper, the length of the simulated time-series is kept at 1000 ns, so the total number of time steps is $M = 5 \times 10^5$. In order to obtain a reliable statistics, the condition $D! << M$ should be satisfied [34]. Meanwhile, a large embedding dimension D is beneficial to include more information for estimating the quantifiers [33, 34]. As a result, the embedding dimension D is set at 7 during the calculation of PE in this work.

3. Results and discussion

The rate-equation model in Eqs. (1)-(4) is expressed using the complex field amplitudes with respect to an optical frequency, in which the free-running optical frequencies for the two linear polarizations of the VCSEL equal $\pm(\gamma_p - \alpha\gamma_a)/2\pi = \pm 1.5$ GHz when the steady-state condition is satisfied [31]. The FBG coupling coefficient $\kappa_B = 100$ m^{-1} corresponds to an approximate full

#238400 - $15.00 USD Received 20 Apr 2015; revised 29 May 2015; accepted 30 May 2015; published 3 Jun 2015

width at half-maximum (FWHM) reflection bandwidth of 6.6 GHz, which is sufficiently broad for reflecting both polarizations if the detuning is set at $f_m = 0$. The peak reflectivity of the FBG is over 0.9, while the amount of feedback light is further controlled by the feedback rate η.

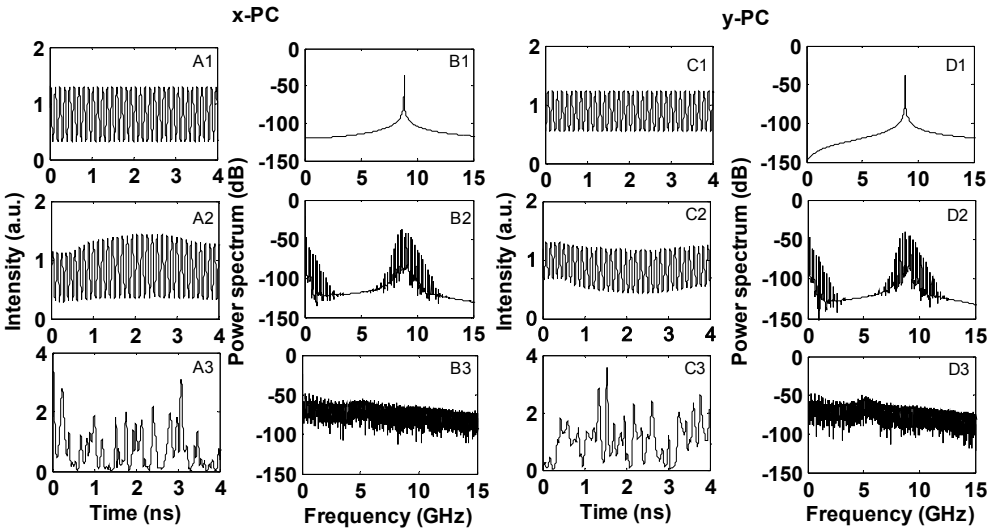

Fig. 2. Polarization-resolved outputs of the VCSEL under FBG feedback. Columns A and C: time-series for the individual polarizations. Columns B and D: power spectra for the individual polarizations. The feedback rate is set to $\eta = 0$ (Row 1), 0.45 ns^{-1} (Row 2), and 12 ns^{-1} (Row 3). The feedback has no detuning.

Figure 2 displays the results of emissions of the VCSEL that are polarization-resolved into the *x*-PC and the *y*-PC, as labeled. The emission intensity time series (Columns A and C) and the corresponding power spectra (Columns B and D) are shown under different feedback ratesη. For $\eta = 0$ in Row 1, the VCSEL is free-running without any feedback. The output of the VCSEL is elliptically polarized due to co-existent *x*-PC and *y*-PC, which are both in periodic oscillations at about 9 GHz. The behavior is qualitatively in consistency with previous numerical results on the solitary VCSEL with a proper bias current [35]. For $\eta = 0.45$ ns^{-1} in Row 2, the oscillations for both polarizations are further modulated by a frequency component of about 0.2 GHz, resulting in a quasi-periodic state. For $\eta = 12$ ns^{-1} in Row 3, both *x*- and *y*-PCs oscillate chaotically. The power spectra show the signal floors being raised much, while the time-series appear to vary erratically. Careful examination of the power spectra does give some peaks at multiples of 0.33 GHz, especially for low frequencies, as expected from the round-trip feedback delay of $\tau = 3$ ns.

When the VCSEL is in chaos, the TD signatures are much affected by the feedback rate η. Figure 3 shows the numerical results for feedback rates $\eta = 40$ ns^{-1} (Row 1), 30 ns^{-1} (Row 2), and 20 ns^{-1} (Row 3). The correlation functions and permutation entropies (PEs) are computed from the intensity time-series of the two linear polarizations. Columns A and C show the SFs against Δt for *x*-PC and *y*-PC, respectively; whereas Column E show the XF between *x*-PC and *y*-PC. Columns B and D show PEs against τ_e for *x*-PC and *y*-PC, respectively. The round-trip feedback delay is fixed at $\tau = 3$ ns. The FBG is centered at the average free-running frequencies of the two polarizations with $f_m = 0$ for the red curves.

#238400 - $15.00 USD Received 20 Apr 2015; revised 29 May 2015; accepted 30 May 2015; published 3 Jun 2015

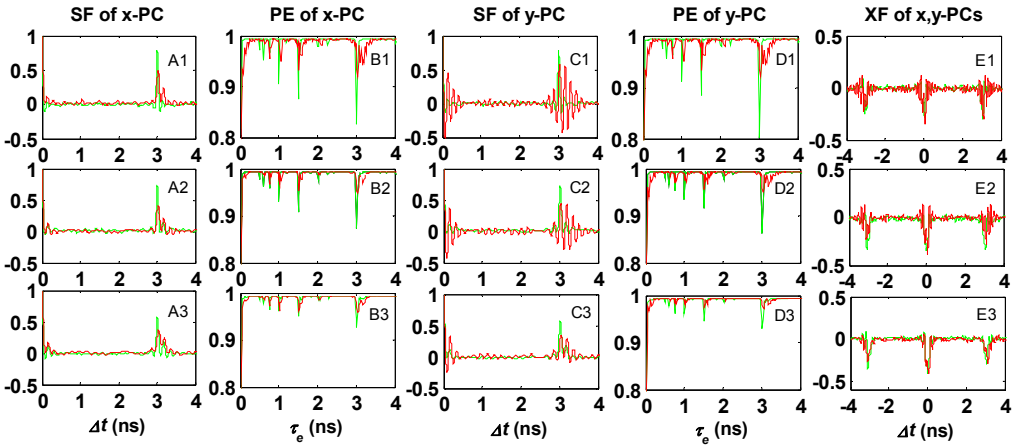

Fig. 3. Polarization-resolved time-delay signatures at zero detuning. Columns A and C: self-correlation functions (SFs) for the individual polarizations. Columns B and D: permutation entropies (PEs) for the individual polarizations. Column E: cross-correlation function (XF) between both polarizations. The feedback rate is set to $\eta = 40$ ns^{-1} (Row 1), 30 ns^{-1} (Row 2), and 20 ns^{-1} (Row 3). The feedback is from the FBG with $\kappa_B = 100$ m^{-1} for the red curves, whereas it is from a mirror for the green curves.

For comparison, the FBG is replaced by a mirror for the green curves in Fig. 3 by setting κ_B to infinity in the simulation [32]. The feedback from the mirror leads to clear SFs at $\Delta t = \tau$ in Columns A and C. Such a mirror feedback also gives anticorrelations between the polarizations as observed at $\Delta t = \pm \tau$ in Column E, which are due to competitions between the PCs. Negative spikes in the traces of PEs are also observed at $\tau_e = \tau$ in Columns B and D. These features clearly unveil the information on the TD at τ in spite of the random-like chaotic waveforms emitted by the VCSEL. Upon carefully contrasting the different rows of Fig. 3, the TD signatures are seen to slightly subside when the strong feedback rate is sequentially reduced from 40 ns^{-1} to 30 ns^{-1} and then to 20 ns^{-1}. Observable dependence on the feedback rate is consistent with earlier works on TD signatures [6].

When the FBG is adopted for feedback, the red curves in Fig. 3 shows improved concealment of the TD information. Correlations at $\Delta t = \tau$ in Columns A and C are reduced. Anticorrelations at $\Delta t = \pm \tau$ in Column E are slightly smoothed out. The negative spikes in the PEs at $\tau_e = \tau$ in Columns B and D become less pronounced, though they still deviate from the ideal value of unity. In general, by using the FBG instead of a mirror for feedback, all of the TD signatures presented in Fig. 3 are suppressed [15, 28]. Yet, it is desirable to further eliminate the residual TD signatures.

Further elimination of the residual TD signatures in FBG feedback is enabled by adjusting f_m while keeping η constant. Figure 4 shows the results for the chaos outputs at $\eta = 20$ ns^{-1} as in the red curves in Row 3 of Fig. 3, except $f_m = -15$ GHz (Row 1) and 15 GHz (Row 2). Contrasting Row 3 of Fig. 3 against Row 1 and Row 2 in Fig. 4 reveals that the TD signatures at $\Delta t = \pm \tau$ and $\tau_e = \tau$ are nearly eliminated. In other words, the peaks at $\Delta t = \tau$ for the SFs are broadened and suppressed. No sharp valleys in the proximity of $\tau_e = \tau$ are observed in the curves. In fact, for $f_m = \pm 15$ GHz as shown in Fig. 4(F), the mean wavelength of the VCSEL is located at a sideband of the FBG reflection spectrum. The reflectivity drops to the order of 1%, which weakens the feedback and hence reduces the TD signatures. The group delay of the FBG depends on the optical frequency and leads to broadening the TD peaks in the correlation functions as well as the entropy traces [15, 32], thereby effectively obscuring the TD signatures.

#238400 - $15.00 USD Received 20 Apr 2015; revised 29 May 2015; accepted 30 May 2015; published 3 Jun 2015

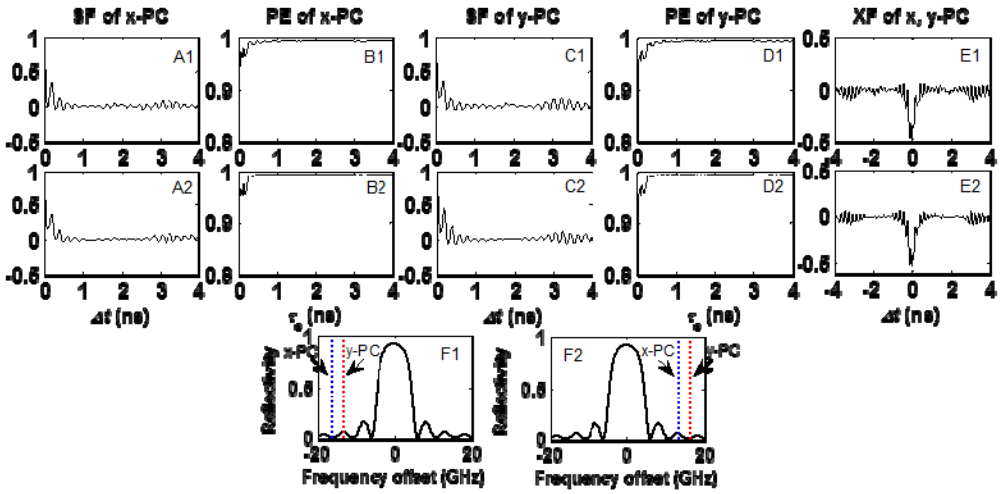

Fig. 4. Polarization-resolved time-delay signatures (A-E) under $\eta = 20$ ns^{-1}. Row 1 and row 2 are for $f_m = -15$ GHz, 15 GHz, respectively. The reflection spectra of FBG under f_m is −15 GHz and 15 GHz are given in F1 and F2, respectively.

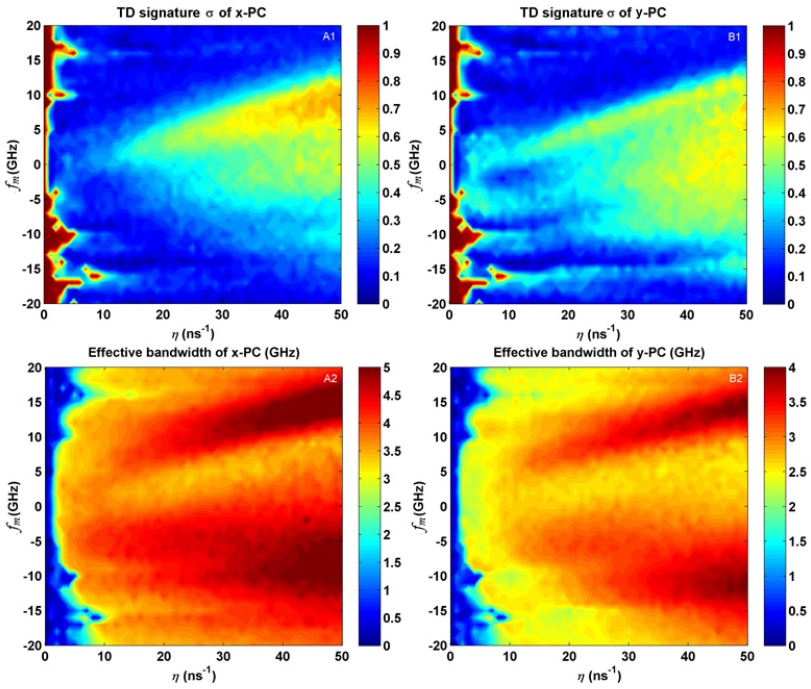

Fig. 5. Polarization-resolved maps of the TD signatures σ from self-correlations (Row 1) and effective bandwidths (Row 2) of the chaotic outputs of the VCSEL under FBG feedback. Column A: x-PC. Column B: y-PC. The maps are shown in the parameter space of η and f_m.

The above results demonstrate that the feedback rate η and the frequency deviation f_m both affect TD signature suppression. Besides the TD signature, the bandwidth is also an important performance index to assess a chaos signal, which is directly related to the transmission rate of messages in chaos secure communication [25] or the bit rate of the random number extracted from an SL-based chaos entropy source [10]. In this work, we use the effective bandwidth to characterize the bandwidths of chaos signals after taking into account that the effective

#238400 - $15.00 USD Received 20 Apr 2015; revised 29 May 2015; accepted 30 May 2015; published 3 Jun 2015

bandwidth, which is obtained by summing up only those discrete spectral segments of the power spectrum accounting for 80% of the total power, is superior to the standard bandwidth for distinguishing the broadband chaotic states from the narrowband periodic oscillations [36]. Figure 5 shows the maps, in the parameter space of (η, f_m), about the TD signatures and the effective signal bandwidths of polarization-resolved outputs from the VCSEL with FBG feedback. For quantification, the TD signature σ is defined as the maximum value of the SFs at Δt in the region of [2 ns, 4 ns] in the maps in Figs. 5(A1) and Fig. 5(B1). The maps for x-PC and y-PC respectively recorded in Figs. 5(A1) and Fig. 5(B1) are quite similar, where regions in deep blue color at positive and negative f_m show successful reduction of the TD signature to around 0.1. It should be pointed out that, for small η, the TD signature σ is nearly equal to 1 while the bandwidth of the power spectrum is very small. These are attributed to stable or periodic oscillatory intensities of the VCSEL for small η. As the feedback rate η increases, the effective bandwidths of the polarization-resolved outputs from the VCSEL increase rapidly, which are consistent with the dynamical development from period oscillation into chaos. Obviously, low TD signatures at around 0.1 along with bandwidth of around 4 GHz can be easily achieved simultaneously for both x-PC and y-PC, according to combining the information in the four maps in Fig. 5. In other words, the maps are useful for locating optimal operation parameters to generate chaotic signals with small TD signatures and wide bandwidths.

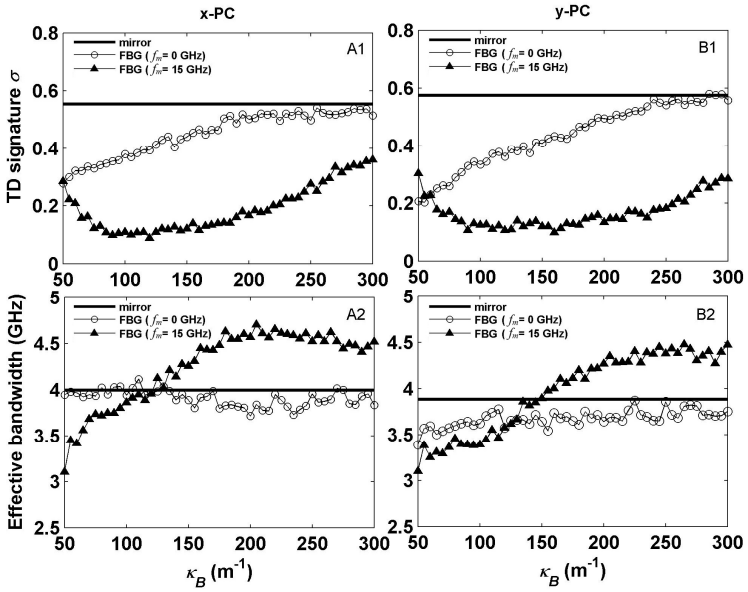

Fig. 6. TD signatures (Row 1) and effective bandwidths (Row 2) of polarization-resolved outputs from the VCSEL. Column A: x-PC. Column B: y-PC. The VCSEL is subject to feedback from mirror (solid lines), FBG under f_m = 0 (circles) and f_m = 15 GHz (triangles), respectively. The magnitude of the coupling coefficient κ_B is varied for the FBG. The feedback rate is fixed at η = 20 ns^{-1}.

In order to emphasize the advantages of using FBG instead of mirror for feedback, we compare VCSEL with FBG feedback and with conventional mirror feedback in Fig. 6. The TD signature σ and the effective bandwidth are, respectively, plotted in Rows 1 and 2 of Fig. 6. The results for the x-PC and y-PC are shown in Columns A and B, respectively. The feedback using FBG is examined as κ_B varies, where f_m is set at 0 and 15 GHz for the circles and triangles, respectively. As references, the solid lines in Fig. 6 indicate the values when κ_B is set to infinity in realizing mirror feedback into the VCSEL. Generally, from Row 1 of Fig. 6, FBG is clearly superior to mirror for suppressing chaotic TD signatures in the VCSEL. Deviating f_m from zero

#238400 - $15.00 USD Received 20 Apr 2015; revised 29 May 2015; accepted 30 May 2015; published 3 Jun 2015

may further conceal the TD signatures. Besides, from Row 2 of Fig. 6, the FBG feedback can even induce chaos with bandwidths exceeding that of mirror feedback. Additionally, it should be pointed out that for VCSELs with polarization rotated feedback, relevant experiments revealed that the TD signatures σ of both two PCs can reach a level of 0.1 for single cavity polarization rotated feedback or even smaller than 0.05 for double-cavity polarization rotated feedback [24]. The above calculations show that adopting FBG feedback can achieve similar effect with polarization rotated feedback in TD signature concealment, and related experimental verification is possible.

4. Conclusions

In summary, the polarization-resolved TD signatures of the chaos outputs from the VCSEL subject to feedback from the FBG have been numerically investigated. Based on the SFM formulism, the intensity time-series for both *x*-PC and *y*-PC are calculated, where self-correlations, cross-correlations, and permutation entropies are used to quantitatively evaluate the TD signatures. The results show that, under suitable operational parameters, the TD signatures of chaos in both polarizations can be suppressed efficiently by the FBG instead of the mirror for feedbacks. With the aid of the maps of TD signatures and effective bandwidths in the parameter space of feedback rates and frequency deviations, two chaotic PCs with both small TD signatures and broad chaotic bandwidths are obtained. Direct comparison between FBG feedback and mirror feedback suggest that the former is much more useful in secure communications due to a better concealment of the TD signature in the chaotic regime. Compared with VCSELs subject to polarization rotated feedback [24] or mutually coupled VCSELs with polarization optical injection [37], in which good TD concealment can be achieved experimentally, such FBG feedback may be relatively simple since there is no need for using optics to rotate the feedback polarizations. We hope this work would be helpful for obtaining high quality dual-polarization chaos signals for some special applications.

Acknowledgments

This work was supported by the National Natural Science Foundation of China under Grant 61178011, Grant 61275116, Grant 61475127, and Grant 61308002, the Postgraduate Research and Innovation Project of Chongqing Municipality under Grant CYB14054, and the Research Grant Council of Hong Kong under Project CityU 110712.

#238400 - $15.00 USD Received 20 Apr 2015; revised 29 May 2015; accepted 30 May 2015; published 3 Jun 2015